

MODELLING AND OPTIMIZATION OF A CPV SYSTEM WITH EQUATORIAL TRACKING

I.S. HERMENEAN¹ I. VIŞA¹ A. DUŢĂ¹
D.V. DIACONESCU¹

Abstract: *The paper presents research on modelling the influence of an equatorial tracking system on the efficiency of a low concentrated Photovoltaic (CPV) system build up of a PV module and two mirrors. This work sets the influences of the tracking system, the tracking accuracy and the geometric parameters on the tracking efficiency of a CPV system. The main objectives of the paper are: to maximize the tracking efficiency of the direct radiation, to minimize the overall size of the CPV system and to compare the equatorial to the previous discussed pseudo-equatorial tracking system. The geometric modelling and the numerical simulations allow the identification of the optimal solutions.*

Key words: *low CPV system, equatorial tracking, tracking efficiency, overall size.*

1. Introduction

To increase the overall efficiency of a photovoltaic system, concentration can be used. Efficiencies even beyond 30% [2] have been registered.

The research focuses on a low concentration system; our aim is to find the influences of the tracking system, the tracking accuracy and the geometric parameters on the tracking efficiency of a low CPV system.

This paper presents the geometric modelling followed by the formulation of the optimal working parameters considering an equatorial tracking system. The simulations were developed considering the geographical location of the Braşov - Romania area, with specific regional

parameters [5]. For concluding results the equatorial tracked CPV system is compared to the same assembly tracked pseudo-equatorial.

The design of the CPV system includes a PV module and two mirrors, symmetrically disposed on the left (M1) and right (M2) side along the length of the PV module, as presented in Figure 1 (similar to [4]).

This paper reports on the pre-dimensioning of the mirrors, according to the PV module dimensions when using an equatorial tracking system. Numerical simulations help in identifying the parameters that influence functionality of the CPV system tracked with an equatorial system compared to a pseudo-equatorial system.

¹ Centre "Product Design for Sustainable Development", *Transilvania* University of Braşov.

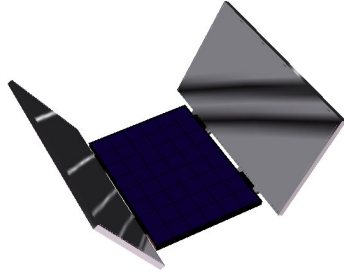


Fig. 1. Low solar concentrating system build up by a photovoltaic module and two lateral disposed mirrors

2. Geometric Modelling and Problem Statement

The goal of our research is to optimize the dimensions of the low CPV (Figure 1) system, identifying the lowest overall size of the system that gains the maximum amount of direct radiation, increasing the efficiency of the system. This followed by the comparison between equatorial and pseudo-equatorial tracking systems.

Considering a given PV module, the parameters that influence the dimensions of the CPV system are, according to Figures 3 and 4: the tracking system (equatorial, pseudo-equatorial or azimuth); the tracking program, defined by the maximum PV incidence angle (ν_M); the inclination angle between the PV-module and the mirror (θ); the ratio between the mirror width and PV module width (kw) and the ratio between the additional length of the mirror and the width of the PV module (kl). The ratio kl shows how much the mirror length increases compared to the PV length, so that the all the reflected radiation falls on the PV module. The ratio kw and kl depend on the values of ν_M and θ .

This paper discusses the case in which the CPV assembly is orientated using an equatorial tracking system.

Following simplifications are assumed in the analysis: (1) the direct radiation on the

PV-module surface, provided by the two mirrors has different values due to the different incidence angles between the reflected rays and the PV module but we considered that this does not influence the proper functioning of the PV module; (2) as a primary assumption we consider that nothing is lost through reflection from the radiation that falls on the mirror.

The corresponding numerical simulations were made considering the Braşov - Romania location (with the latitude $\varphi = 45.6^\circ$ N and the turbidity factor $T_R = 3$ [5]).

The equatorial solar angles, as can be seen in Figure 2, are: the declination angle δ and the hour angle ω , having following expressions, [6]:

$$\delta = 23.45^\circ \sin \frac{360^\circ(N-80)}{365}, \quad (1)$$

$$\omega = 15^\circ(12-T), \quad (2)$$

where, N is the day number in the year and T is the solar time.

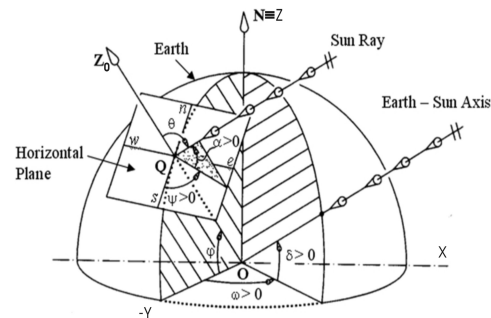


Fig. 2. Global and local reference system and the corresponding sunray angles, used in the calculus of the equatorial sunray angles

The angular displacement of the tracked CPV system is made discontinuously (in steps), so the tracker's equatorial angles (δ , ω) have discrete variations, and are noted with δ^* and ω^* .

The tracking program is designed; a step interval consists of the rotation time (under 1s) and the break, till the next rotation. For equatorial system, the tracking is made seasonally. For the daily movement (ω^*) to have an accurate tracking, as needed for the CPV systems, the maximum PV incidence angle must be smaller than 1° . For this reason, knowing that the sun moves with $15^\circ/\text{hour}$, the tracking step is made at time intervals of 4 minutes. To choose the number of days in a season, and so to determine the elevation movement (δ^*), we start by considering the days where the variation of the declination angle

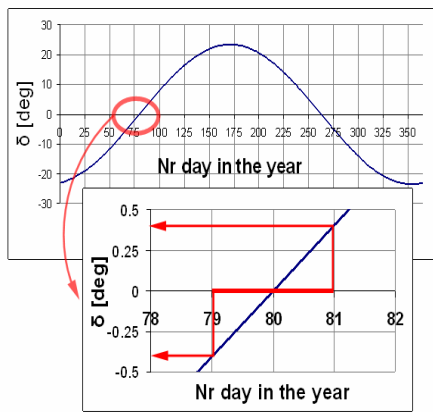


Fig. 3. Declination angle and detail of the three day season

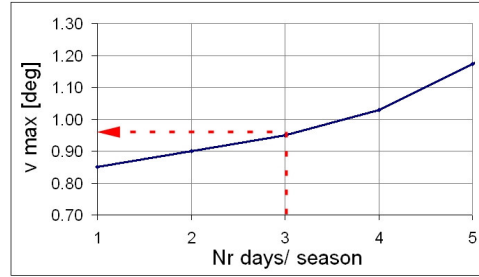


Fig. 4. The variation of the maximum incidence angle compared to the number of days in the season

is maximum (see Figure 3), i.e. proximity of the equinoxes.

Based on the premise that the maximum PV incidence angle is smaller than 1° , Figure 4 is drawn; from which it can be observed that the optimal number of days is reached at seasons build by maximum three days.

The simulations in this paper are made for a three days season ($N = 79...81$) as can be seen from the detail in Figure 3.

To determine the dimensions of the CPV system two ratios are calculated: the width (kw) and longitudinal ratio (kl).

Based on Figures 2, 5 and 6, the main geometric elements of the CPV equatorial tracked system are formulated, and presented in Tables 1 and 2.

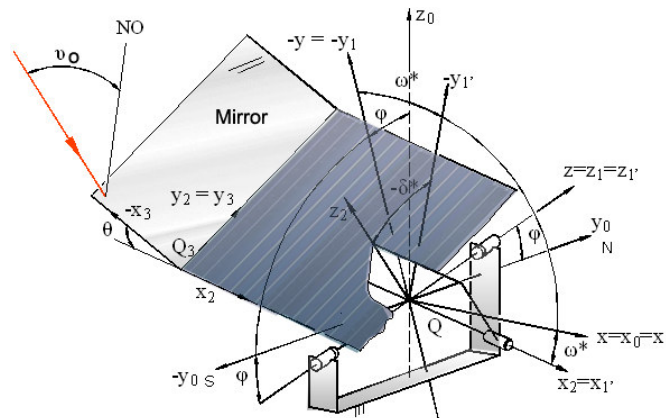


Fig. 5. Geometrical scheme of the CPV system with Equatorial tracking system

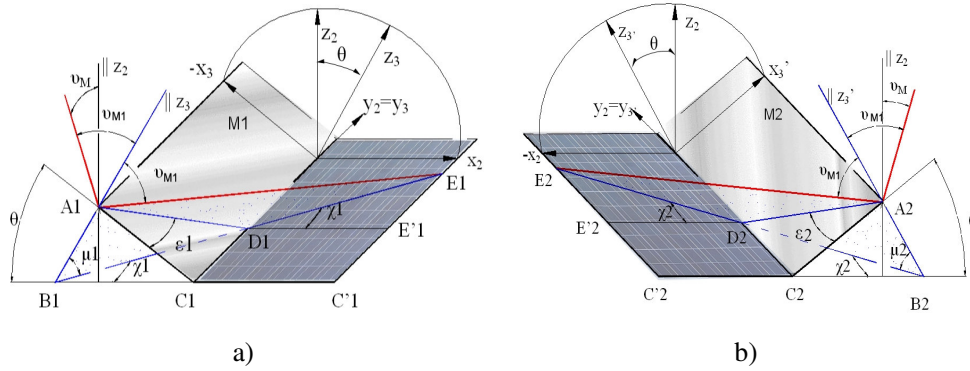


Fig. 6. Geometrical schemes of a low CPV system and the longitudinal deflections of the reflected sunray from the left mirror M1 (a) and from the right mirror M2 (b)

The longitudinal displacement, C'E, of the reflected solar ray is due to the tracking deviation of the elevation angle (δ^*), as Figure 6 presents. From Table 2 we have the expressions (6) for kl and (7) for kw .

Based on these expressions, the curves

presented in Figure 7 are developed, which shows that the width of the mirror increases, due to the θ angle and that the length of the mirror compared to the PV length increases at low values of this angle.

Equations used for estimating the incidence angles (see Figures 2, 5 and 6) Table 1

<p>From Figures 2 and 5: $[e_{sr}]_{xyz} = \begin{bmatrix} \cos \delta \cdot \sin \omega \\ -\cos \delta \cdot \cos \omega \\ \sin \delta \end{bmatrix}$; $[e_{sr}]_{x_0y_0z_0} = T_{xyz-x_0y_0z_0} \cdot [e_{sr}]_{xyz}$; (3), (3a)</p>
<p>$[e_{sr}]_{x_0y_0z_0} = \begin{bmatrix} 1 & 0 & 0 \\ 0 & \sin \varphi & \cos \varphi \\ 0 & -\cos \varphi & \sin \varphi \end{bmatrix} \cdot \begin{bmatrix} \cos \delta \cdot \sin \omega \\ -\cos \delta \cdot \cos \omega \\ \sin \delta \end{bmatrix} = \begin{bmatrix} \cos \delta \cdot \sin \omega \\ -\cos \delta \cdot \cos \omega \cdot \sin \varphi + \sin \delta \cdot \cos \varphi \\ \cos \varphi \cdot \cos \delta \cdot \cos \omega + \sin \varphi \cdot \sin \delta \end{bmatrix}$; (3b)</p> <p>based on Figure 5</p>
<p>$[e_{sr}]_{x_1y_1z_1} = T_{0-1} \cdot [e_{sr}]_{x_0y_0z_0} = \begin{bmatrix} 1 & 0 & 0 \\ 0 & \sin \varphi & -\cos \varphi \\ 0 & \cos \varphi & \sin \varphi \end{bmatrix} \cdot \begin{bmatrix} \cos \delta \cdot \sin \omega \\ -\cos \delta \cdot \cos \omega \cdot \sin \varphi + \sin \delta \cdot \cos \varphi \\ \cos \varphi \cdot \cos \delta \cdot \cos \omega + \sin \varphi \cdot \sin \delta \end{bmatrix} =$ $= \begin{bmatrix} \cos \delta \cdot \sin \omega \\ -\cos \delta \cdot \cos \omega \\ \sin \delta \end{bmatrix}$; (3c)</p> <p>see Figure 5</p>
<p>$[e_{sr}]_{x_1y_1z_1} = T_{1-1} \cdot [e_{sr}]_{x_1y_1z_1} = \begin{bmatrix} \cos \omega^* & \sin \omega^* & 0 \\ -\sin \omega^* & \cos \omega^* & 0 \\ 0 & 0 & 1 \end{bmatrix} \cdot \begin{bmatrix} \cos \delta \cdot \sin \omega \\ -\cos \delta \cdot \cos \omega \\ \sin \delta \end{bmatrix} = \begin{bmatrix} \cos \delta \cdot \sin(\omega - \omega^*) \\ -\cos \delta \cdot \cos(\omega - \omega^*) \\ \sin \delta \end{bmatrix}$; (3d)</p> <p>see Figure 5</p>

$$\begin{aligned}
[e_{sr}]_{x_2, y_2, z_2} &= T_{1-2} \cdot [e_{sr}]_{x_1, y_1, z_1} = \begin{bmatrix} 1 & 0 & 0 \\ 0 & \sin \delta^* & \cos \delta^* \\ 0 & -\cos \delta^* & \sin \delta^* \end{bmatrix} \cdot \begin{bmatrix} \cos \delta \cdot \sin(\omega - \omega^*) \\ -\cos \delta \cdot \cos(\omega - \omega^*) \\ \sin \delta \end{bmatrix} = \\
&= \begin{bmatrix} \cos \delta \cdot \sin(\omega - \omega^*) \\ -\sin \delta^* \cdot \cos \delta \cdot \cos(\omega - \omega^*) + \cos \delta^* \cdot \sin \delta \\ \cos \delta^* \cdot \cos \delta \cdot \cos(\omega - \omega^*) + \sin \delta^* \cdot \sin \delta \end{bmatrix}; \quad (3e)
\end{aligned}$$

For M1 (see Figure 6a)

$$\begin{aligned}
[e_{sr}]_{x_3, y_3, z_3} &= T_{2-3} \cdot [e_{sr}]_{x_2, y_2, z_2} = \begin{bmatrix} \cos \theta & 0 & -\sin \theta \\ 0 & 1 & 0 \\ \sin \theta & 0 & \cos \theta \end{bmatrix} \begin{bmatrix} \cos \delta \cdot \sin(\omega - \omega^*) \\ -\sin \delta^* \cdot \cos \delta \cdot \cos(\omega - \omega^*) + \cos \delta^* \cdot \sin \delta \\ \cos \delta^* \cdot \cos \delta \cdot \cos(\omega - \omega^*) + \sin \delta^* \cdot \sin \delta \end{bmatrix} = \\
&= \begin{bmatrix} \cos \theta \cdot \cos \delta \cdot \sin(\omega - \omega^*) - \sin \theta (\cos \delta^* \cdot \cos \delta \cdot \cos(\omega - \omega^*) + \sin \delta^* \cdot \sin \delta) \\ -\sin \delta^* \cdot \cos \delta \cdot \cos(\omega - \omega^*) + \cos \delta^* \cdot \sin \delta \\ \sin \theta \cdot \cos \delta \cdot \sin(\omega - \omega^*) + \cos \theta (\cos \delta^* \cdot \cos \delta \cdot \cos(\omega - \omega^*) + \sin \delta^* \cdot \sin \delta) \end{bmatrix}; \quad (3f)
\end{aligned}$$

For M2 (see Figure 6b)

$$\begin{aligned}
[e_{sr}]_{x_3, y_3, z_3} &= T_{2-3} \cdot [e_{sr}]_{x_2, y_2, z_2} = \begin{bmatrix} \cos \theta & 0 & \sin \theta \\ 0 & 1 & 0 \\ -\sin \theta & 0 & \cos \theta \end{bmatrix} \begin{bmatrix} \cos \delta \cdot \sin(\omega - \omega^*) \\ -\sin \delta^* \cdot \cos \delta \cdot \cos(\omega - \omega^*) + \cos \delta^* \cdot \sin \delta \\ \cos \delta^* \cdot \cos \delta \cdot \cos(\omega - \omega^*) + \sin \delta^* \cdot \sin \delta \end{bmatrix} = \\
&= \begin{bmatrix} \cos \theta \cdot \cos \delta \cdot \sin(\omega - \omega^*) + \sin \theta (\cos \delta^* \cdot \cos \delta \cdot \cos(\omega - \omega^*) + \sin \delta^* \cdot \sin \delta) \\ -\sin \delta^* \cdot \cos \delta \cdot \cos(\omega - \omega^*) + \cos \delta^* \cdot \sin \delta \\ -\sin \theta \cdot \cos \delta \cdot \sin(\omega - \omega^*) + \cos \theta (\cos \delta^* \cdot \cos \delta \cdot \cos(\omega - \omega^*) + \sin \delta^* \cdot \sin \delta) \end{bmatrix}; \quad (3g)
\end{aligned}$$

For M1 the incidence angle becomes:

$$\cos \nu_{M1} = \sin \theta \cdot \cos \delta \cdot \sin(\omega - \omega^*) + \cos \theta (\cos \delta^* \cdot \cos \delta \cdot \cos(\omega - \omega^*) + \sin \delta^* \cdot \sin \delta); \quad (4)$$

For M2 the incidence angle becomes:

$$\cos \nu_{M2} = -\sin \theta \cdot \cos \delta \cdot \sin(\omega - \omega^*) + \cos \theta (\cos \delta^* \cdot \cos \delta \cdot \cos(\omega - \omega^*) + \sin \delta^* \cdot \sin \delta). \quad (4a)$$

Equations used for estimating the longitudinal and width ratio (see Figure 6) Table 2

$C'E = CD + E'E$, $CD = AC \cdot \tan \varepsilon$, $EE' = DE \cdot \sin \chi$;	(5), (5a), (5b)
$DE = AC \left(\frac{\sin \theta \cdot \sin \nu_0}{\sin(\nu_0 - \mu)} - \frac{\cos \varepsilon}{\cos(90 - \mu)} \right)$;	(5c)
$\tan \varepsilon = \frac{-\sin \delta^* \cdot \cos \delta \cdot \cos(\omega - \omega^*) + \cos \delta^* \cdot \sin \delta}{\cos \theta \cdot \cos \delta \cdot \sin(\omega - \omega^*) + \sin \theta (\cos \delta^* \cdot \cos \delta \cdot \cos(\omega - \omega^*) + \sin \delta^* \cdot \sin \delta)}$;	(5d)
$\tan \chi = \tan \varepsilon \cdot \cos \theta$, $\tan \mu = \frac{1}{\tan \theta \cdot \cos \varepsilon}$;	(5e), (5f)
$k_l = \frac{2 \cdot C'E}{CC'}$, $k_w = \frac{AC}{CC'} = \frac{\cos \varepsilon \cdot \sin(\nu_{M1,2} - \mu)}{\cos \nu_{M1,2} \cdot \cos \chi}$.	(6), (7)

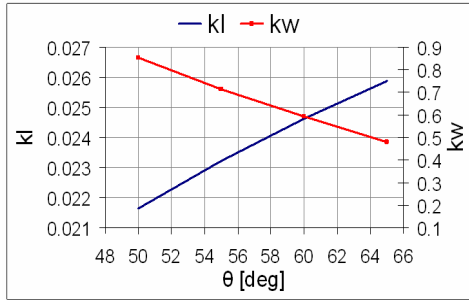


Fig. 7. The Variations of kw and kl

From Figure 7 it can be observed that the ratios kw and kl have reasonable minimum dimensions.

3. Numerical Simulations and Results

For the θ angle, there were considered different values: 50° , 55° , 60° and 65° , chosen from Figure 7.

The variations of the sun angles (δ and ω) and the PV angles (δ^* and ω^*) are shown in the diagrams in Figure 8 during the season's middle day $N = 80$.

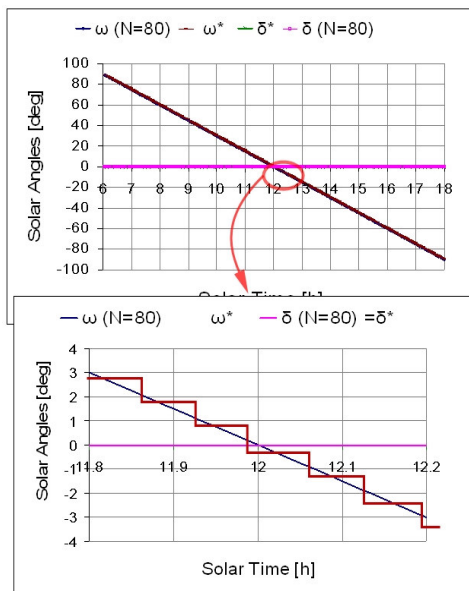


Fig. 8. The variation of the solar angles

With the computed solar angles are estimated the variations of the incidence angles that fall on the PV- surface, i.e. the angles of the solar ray and of the reflected rays from the mirrors (Figure 9).

The amount of direct solar radiation is computed with the equations [3]:

$$B_S = B_0 \exp[-T_R / (0.9 + 9.4 \sin \alpha)], \quad (8)$$

$$B_0 = 1367 [1 + 0.03 \cos(0.98N - 2.27)], \quad (8a)$$

where B_S is the direct solar radiation, T_R is the turbidity factor [3], α is the altitude angle and N - day number in a year.

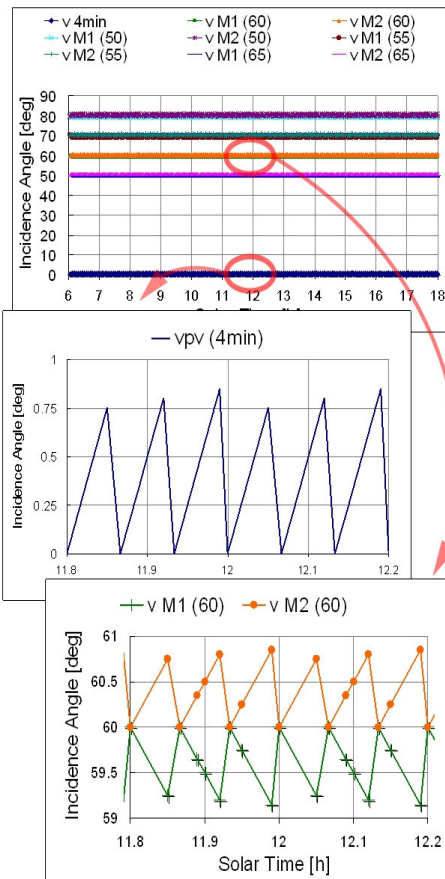


Fig. 9. The variation of the incidence angle on the PV, with different values of θ

The radiation that falls normal on the PV, due to the sun ray reflection on the mirrors, is computed using the Lambert Law, as follows:

$$B_{cpv_{M1,2}} = B_s \cos(v_{M1,2}), \quad (9)$$

where $v_{M1,2}$ is the incidence angle of the reflected ray with the normal of the PV module.

The expression (9) gives the average equivalent radiation that falls normal on the entire PV-module from the reflected rays of each mirror (M1 and M2).

The total radiation that falls on the PV as reflection from the mirrors is the sum between the radiation from mirror one and respectively mirror two:

$$B_{cpv} = \sum B_{cpv_{M1,2}}. \quad (10)$$

In Figure 10 is presented the variation of the total direct radiation received normal on the PV module at different values of the θ angle; the values written above each curve represent the absolute tracking efficiency (the amount of radiation that falls on the PV module, direct from the sun and reflected from the mirrors, compared to the available radiation) of the CPV system tracked by the equatorial system.

Comparing to the pseudo-equatorial tracking system, approached in previous work [1], the absolute tracking efficiencies in the case of equatorial tracked CPV system have practically the same values (see Figure 11). According to Figure 10, and highlighted in Figure 11, the highest tracking efficiencies are reached at high θ values, which means a big overall size of the CPV system.

The difference is made by the number of tracking steps needed by each tracker to keep the maximum PV incidence angle (v_M) under 1° . The pseudo-equatorial needs

almost the double amount of tracking steps compared to the equatorial tracker to reach this accuracy.

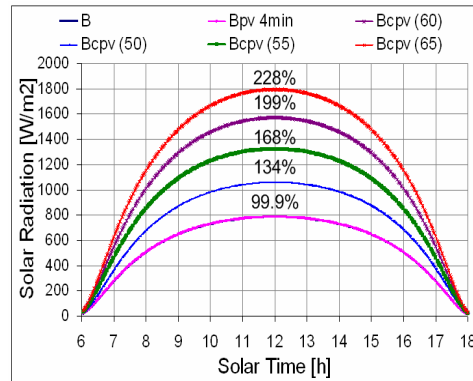


Fig. 10. Total direct solar radiation variations that fall on the PV-module, at different values of angle θ and afferent absolute tracking efficiencies

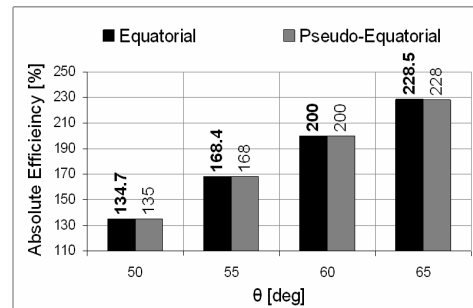


Fig. 11. The absolute efficiency of the CPV system at different values of angle θ

4. Conclusions

1. The main objectives of the paper are:
 - a) to optimize the dimensions of the low CPV system;
 - b) to identify the lowest overall size of the system that gains the maximum amount of direct radiation;
 - c) to increase the efficiency of the system;
 - d) the comparison between equatorial and pseudo-equatorial tracking systems.

2. The parameters that influence the tracking efficiency and the overall size of the CPV system tracked are: the tracking program accuracy and the inclination angle between the mirror and PV module (θ); the overall size of the CPV system is described by the width ratio kw and the longitudinal ratio kl .

3. The overall size described by the width ratio kw increases with the angles θ , while the overall size described by the kl ratio decreases with θ angle.

4. The comparative analysis between the two types of tracker (equatorial and pseudo-equatorial) the absolute efficiency has practically the same values.

5. The number of tracking steps needed by each tracker to keep the maximum PV incidence angle under 1° is almost double in the case of pseudo-equatorial tracker. Another advantage of the equatorial system is a simpler working mechanism, having the possibility of changing the elevation angle seasonally. Furthermore the motor for elevation tracking is less solicited due to fewer movements.

6. Using the equatorial tracking, a simpler tracking program can be obtained (i.e. simpler command and control system).

References

1. Hermenean, I.S., et al.: *Modelling and Optimization of a Concentrated Hybrid Photovoltaic System with Pseudo-Equatorial Tracking*. In: CD-ROM Proc. of EVER Conference, Monaco, March 2010.
2. Klotz, F.H.: *European Photovoltaic V-Trough Concentrator System with Gravitational Tracking*. In: Proc. of the 16th EU PVSEC, Glasgow, UK, May 2000, p. 2229-2235.
3. Meliss, M.: *Regenerative Energiequellen*. Berlin. Springer, 1997, p. 5-7.
4. Reis, F., et al.: *Power Generation and Energy Yield using Doublesun Photovoltaic Solar Concentration*. In: Proc. 24th EU PVSEC, Hamburg, Germany, September 2009, p. 803-806.
5. Vătăşescu, M., et al.: *Atmospheric Pollution Evaluation in Braşov Romania Based on Turbidity Factor Analysis*. Accepted for IC-ANMBES Conf., Braşov, Romania, March 2010.
6. Vişa, I., et al.: *On the Incidence Angle Optimization of the Dual-Axis Solar Tracker*. In: 11th Inter. Research/Expert Conf. TMT, Hamammet, Tunisia, September 2007, p. 1111-1114.